

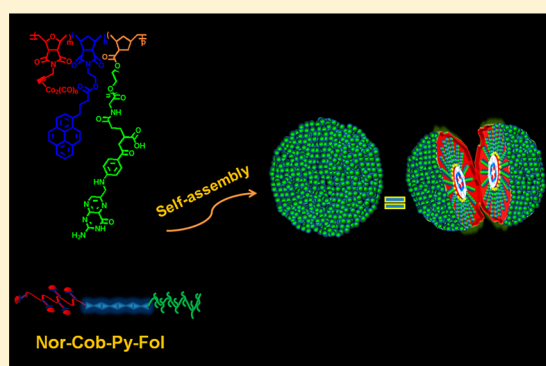
Site-Specific Amphiphilic Magnetic Copolymer Nanoaggregates for Dual Imaging

Saikat Mukherjee,[†] Himadri Dinda,[†] Litesh Shashank,[†] Ipsita Chakraborty,[‡] Rangeet Bhattacharyya,[‡] Jayasri Das Sarma,[§] and Raja Shunmugam^{*,†}

[†]Polymer Research Centre, Department of Chemical Sciences, [‡]Department of Physical Sciences, and [§]Department of Biological Sciences, Indian Institute of Science Education and Research Kolkata, Mohanpur Campus, Mohanpur – 741 246, Dist. Nadia, West Bengal, India

S Supporting Information

ABSTRACT: Molecular imaging along with combinations of imaging modalities can provide a thorough understanding of disease, in particular, tumors. Magnetic resonance imaging (MRI) offers exceptional tissue contrast and resolution; whereas optical imaging provides high sensitivity. Hence a norbornene based copolymer (Nor-Cob-Py-Fol) is reported in this paper as a dual-imaging agent. Nor-Cob-Py-Fol having Co²⁺ complex, pyrene and poly(ethylene glycol) derived folate, have been synthesized using ring-opening metathesis polymerization (ROMP). All the monomers and polymers are characterized by ¹H NMR, IR, GPC, and TGA techniques. The morphology of the copolymer nanoaggregates has been evaluated with DLS, TEM, and SEM techniques. The functionalization of Co²⁺ to the polymer is monitored by FTIR, ¹H NMR, and ¹³C NMR spectroscopy. Furthermore, the presence of Co²⁺ in the nanoaggregates is confirmed by the EDX (SEM) technique. To prove the MRI capabilities nature of copolymer nanoaggregates, NMR experiment is performed at room temperature. Cell viability studies suggest the biocompatibility nature of the copolymer. Flow cytometry as well as epifluorescence microscope experiments clearly demonstrate the dual-imaging ability of the newly designed copolymer. The much higher relaxivity ratio (r_2/r_1) of the present method clearly establishes the superiority of our system as one of the best contrast agents known to the practitioners of magnetic resonance imaging.



INTRODUCTION

Cancer detection at the primary level is the key factor for successful cancer therapy, which improves the survival rates.^{1,2} To detect the primary level, multimodal bioimaging has been emerging as a promising diagnosis technique which is also having broad clinical application.^{1,2} The site specific delivery of such imaging agents has become an important area of research. There are few diagnostic techniques available in which magnetic resonance imaging (MRI) is a powerful diagnostic technique which gives the clear insight on the damage of tissue and cells.^{3–5} There are two types of contrast agents available in the literature: one is T_1 active and another is T_2 active. Magnetic metal ion or particle causes shortening of T_1 (longitudinal relaxation) (e.g., Gd³⁺) known as T_1 active MRI contrast agent and another kind of contrast agent dealing with the shortening of T_2 (transverse relaxation), (e.g., Co²⁺, Fe₃O₄) known as T_2 active MRI agent.³ There are number of literature available where Co²⁺ based nano particle systems that have been used as a T_2 active contrast agent, meaning, these systems cause for the shortening of T_2 (by increasing r_2) and resulting in a darkening effect, hence known as negative contrast agent.^{3,6} Franchini and co-workers⁷ have reported the CoFe₂O₄ nanoparticle for MRI imaging. Britton and co-workers have demonstrated Co²⁺ based magnetic complex

which is MRI active.⁶ Morrow and co-workers have also proven the Co²⁺ based metal complex as a MRI contrast agent.⁸ But all the existing examples deal with either simple magnetic nano particle systems or the magnetic nano particle encapsulated to the polymeric systems.^{9–12} Furthermore, the quantitative amounts of magnetic particle attached or encapsulated to these polymeric systems as well as the solubility are always a problematic issue for the existing systems.^{9,10} Therefore, pressing need for a system where the magnetic nanoparticle preferably attached to the polymer covalently.

Tew and co-workers have pioneered in attaching the cobalt carbonyl to the terminal alkyne group to get the covalently attached cobalt complex.¹³ It has been also reported that norbornene derived cobalt homopolymer is super paramagnetic in nature.¹⁴ So it has been envisioned by us that if this homopolymer can be stabilized in the biological environment, then it can be used as a potential imaging agent. But it is also well-known fact that it is always very difficult to stabilize the cobalt-based material inside our body as upon contact with water, cobalt

Received: August 2, 2015

Revised: September 7, 2015

carbonyl gets precipitated immediately.¹⁵ Because of this problem, it is very rare to see a cobalt-based nanocarrier systems for biological application. Because of these issues, the observed r_2/r_1 values of the existing systems are not greater than 50 to best of our knowledge.¹⁶

In vivo imaging and diagnostics is also dominated by optical imaging probes.¹⁷ Several methods are available in the literature to incorporate emissive probes in the nanostructures. The noncovalent encapsulation approach is limited by out-diffusion of the emissive small molecules.¹⁸ Alternatively, covalent assembly of the emissive molecule within nanostructure core is most promising nanomaterials for theranotics.¹⁹ Thus, a new class of polymer based nanoaggregates that can have highly fluorescent probe is in high demand.²⁰

Molecular imaging provides a better understanding of tumor processes.¹⁶ Hence, the combination of polymer based nanomaterials with molecular imaging can provide a deeper understanding of disease.²¹ If the optical imaging techniques claim their superiority for the high sensitivity, then MRI techniques are advantageous for greatest resolution and isotropic depth of imaging.²² Motivated from this, herein, for the first time, we have designed a norbornene derived cobalt copolymer which is super paramagnetic in nature and also stable in biological conditions. We have synthesized norbornene derived triblock copolymer which is consisting of cobalt, pyrene, and folate motifs as pendent functionalities. Poly(ethylene glycol) has been used to make the system water-soluble as well as for the longer blood circulation.²³ Recent reports suggests that the targeted accumulation of nanocarriers in tissue is much favorable for the imaging as opposed to accumulation due to traditional EPR effect.²⁴ Hence, the presence of folate functionality makes the system to accumulate in tissue effectively by using site specific folate receptor.²⁵ To make the system fluorescence active, we have introduced pyrene motifs. Because of this, the internalization of the newly designed nanocarrier shall be clearly monitored under the epifluorescence microscope during cell *in vitro* studies.²⁶ Both pyrene and cobalt makes the nanocarrier as dual-imaging system. The relaxivity study confirms the system as a T_2 weighted MRI contrast agent having unusually high relaxivity ratio ($r_2/r_1 = 160$). Flow cytometry analysis confirms the greater internalization of the newly designed nanocarrier under the magnetic field.^{27,28} This newly designed water-soluble fluorescent polymer is stable over more than six months in water which makes our system best compared to other similar examples available in the literature.¹⁶ To best of our knowledge this is the report which demonstrates the efficient method to make covalently attached Co^{2+} to the polymeric backbone along with a fluorescent probe for the dual imaging. This is the unique system where, a dual-imaging has been elegantly demonstrated for a polymeric system with greater r_2/r_1 values as well as highly emissive properties.

■ EXPERIMENTAL SECTION

Synthesis of Mono 1. In a dry two neck round bottomed flask, 0.8 g of **2** (0.001586 mol) was dissolved in dry DCM. N_2 gas was passed through the solution, and the flask was kept in an ice bath. In another flask 1.1 g of cobalt carbonyl (0.00317 mol) was dissolved in dry DCM. This was added dropwise fashion to the solution containing **2**. After that the reaction mixture was stirred for 2 h in room temperature. After completion of reaction (monitored by TLC) the solvent was removed using rota vapor. The product was recovered by precipitating it from pentane. Pure product was collected after doing column chromatography separation process. (SiO_2 , DCM, acetone). Yield: 0.63 g (0.00142 mol, 90%). ^1H NMR (CDCl_3 , 500 MHz), δ (ppm): 6.5 (s, 2H), 5.2 (s,

2H), 4.8 (s, 2H), 2.9 (s, 2H), 6.0 (s, 1H) (Figure S5). ^{13}C NMR (CDCl_3 , 500 MHz), δ (ppm): 200, 175, 136, 88, 81, 72, 47, 41 (Figure S6). ESI MS calculated for $\text{C}_{19}\text{H}_{15}\text{Co}_2\text{NO}_9$ [$\text{M} + \text{H}$] $^+$, 520.19; observed, 520.21.

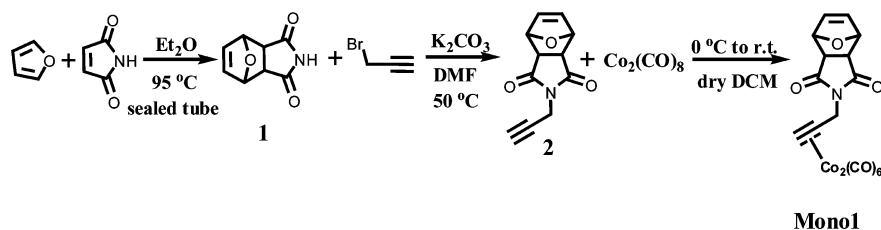
Synthesis of Mono 2. A 950 mg (3.29 mmol) sample of pyrene butyric acid was dissolved in dry DCM. Then, 850 mg (4.08 mmol) of DCC was added to it and the reaction stirred for 1 h. Then 650 mg (3.14 mmol) of **1** and 50 mg of DMAP was added to it and stirred for 24 h. After completion of the reaction, the reaction mixture was filtered and washed with water and concentrated. Column chromatography separation was done to get the pure product as white powder (EtOAc–hexane as eluent). Yield: 1 g (70%, 2.3 mmol) ^1H NMR ($\text{DMSO}-d_6$, 500 MHz), δ (ppm): 8.35 (d, 1H), 8.25 (m, 2H), 8.21 (q, 2H), 8.12 (d, 2H), 8.05 (t, 1H), 7.9 (d, 1H), 6.1 (t, 2H), 4.1 (t, 2H), 3.6 (t, 2H), 2.84 (t, 2H), 2.55 (d, 2H), 2.36 (t, 2H), 1.97 (m, 2H), 1.03–1.08 (m, 2H) (Figure S9). ^{13}C NMR ($\text{DMSO}-d_6$, 500 MHz), δ (ppm): 177, 172, 137.5, 136, 130.8, 130.4, 129.3, 128.1, 127.5, 127.4, 127.2, 126.5, 126.1, 125, 124.8, 124.2, 124.1, 123.5, 60, 47.1, 44.3, 42.1, 37, 33, 31.8, 26.5 (Figure S10). ESI MS calculated for $\text{C}_8\text{H}_7\text{NO}_3$ [$\text{M} + \text{H}$] $^+$, 477.19; observed, 477.21.

Synthesis of Mono 3. First, 0.1 g of folic acid (0.000226 mol) was dissolved in dry DMSO and 0.00513 g of DCC (0.000249 mol) was added to it. The reaction mixture was stirred vigorously for 1 h. Then 0.36 g of **6** (0.000215 mol) was added to the reaction mixture along with the DMAP (0.0000226 mol). The reaction mixture was stirred vigorously for 24 h at room temperature. After completion of the reaction the reaction mixture was precipitated in cold diethyl ether. The precipitate was re dissolved in DCM and again reprecipitated in diethyl ether for three times to obtain the **Mono 3**. Yield: 285 mg (0.000135 mol, 60%). ^1H NMR ($\text{DMSO}-d_6$, 500 MHz), δ (ppm): 11.3 (s, 1H), 9.9 (s, 2H broad), 8.66 (s, 1H), 8.624 (t, 1H), 8.18 (s, 1H), 8.1 (d, 1H), 7.4 (2H, dd), 6.5–6.7 (d, 2H), 6.14 (d, 2H), 4.57 (t, 2H), 4.50–4.54 (m, 2H), 4.43–4.4 (m, 2H), 3.6 (s, broad), 2.9 (s, 2H), 2.19–2.28 (m, 2H), 2.30–2.33 (t, 2H), 2.0–2.07 (m, 2H), 1.86–1.94 (m, 2H), 1.50–1.56 (m, 2H), 1.2–1.6 (m, 2H) (Figure S16). Mass observed in MALDI 1131.098 (Figure S21).

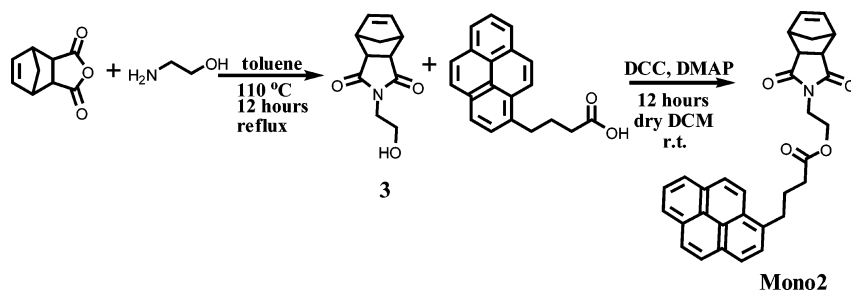
Preparation of Grubbs' Third Generation (G-3) Catalyst. Freshly prepared Grubbs' third generation catalyst²⁹ was used for all the polymerization reactions. In details, desired amount of Grubbs' second generation catalyst (G-2) was placed in a glass vial. To this was added 2-bromopyridine and the reaction stirred for 2 min. The immediate green coloration of the reaction mixture confirmed the formation of catalyst. The product was precipitated from pentane. The whole reaction was carried out inside the glovebox under the nitrogen atmosphere.

Polymerization Procedure. The polymerization was done by following previously reported literature.^{27,30,31} A known amount of three monomers were weighed separately and taken in a 15 mL glass vial. Then desired amount of Grubbs' third generation catalyst was weighed in a separate vial and dissolved in minimum amount of dry CH_2Cl_2 . Polymerization was done in an inert atmosphere inside the glovebox. 2.1 mg of catalyst was transferred to the vial containing 25 mg (0.05 mmol) of **Mono 1** via syringe. The reaction was allowed to stir for 10 min for complete polymerization. An aliquot of sample was quenched with ethyle vinyl ether, precipitated in pentane and taken for GPC analysis. Gel permeation chromatography (GPC) was done in tetrahydrofuran (flow rate = 1 mL/min). The molecular weight of the **Macroinitiator 1 (Nor-Cob)** was measured as $M_n = 8000$ Da (PDI = 1.04) by using poly(methyl methacrylate) standard. Then 120 mg (0.125 mmol) of the second monomer (**Mono 2**) was added to the reaction vial after dissolving it in minimum quantity of dry CH_2Cl_2 . The reaction mixture was stirred for 8 h and an aliquot was taken for GPC analysis. The molecular weight of **Macroinitiator 2 (Nor-Cob-Py)** was measured $M_n = 17000$ Da (PDI = 1.09) by using polymethyl methacrylate standard. Finally 130 mg (0.102 mmol) of **Mono 3** was added to the reaction vial and stirred until polymerization complete. Then the reaction mixture was quenched with ethyl vinyl ether (1 mL). An aliquot was taken for GPC analysis, and the remaining product was precipitated from pentane, dissolved again in THF, passed through neutral alumina to remove the catalyst, and precipitated again from pentane to get a pure triblock copolymer (**Nor-Cob-Py-Fol**). The molecular weight of the final

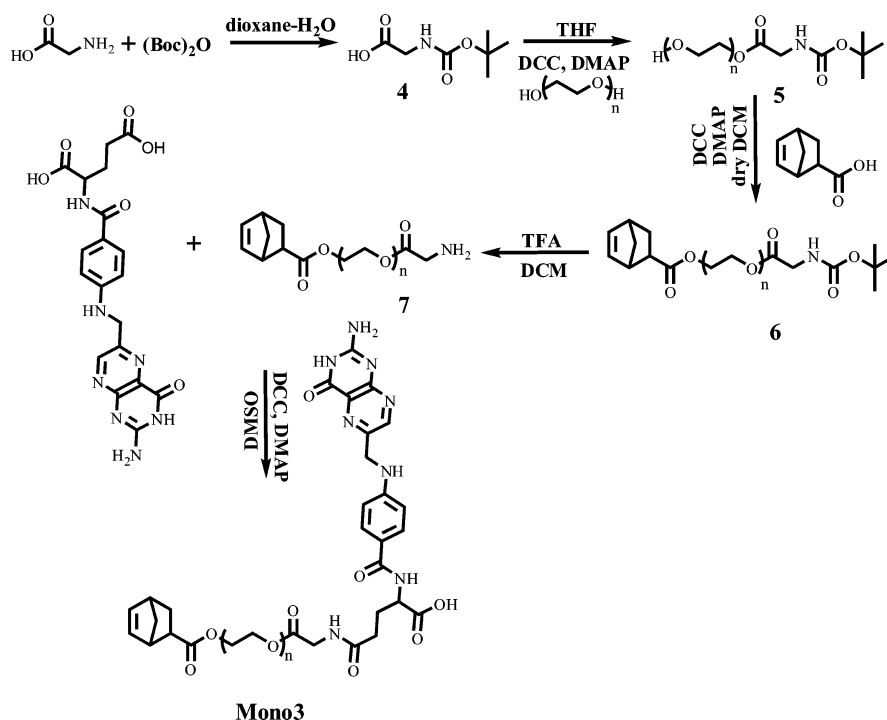
Scheme 1. Synthesis of Mono 1



Scheme 2. Synthesis of Mono 2



Scheme 3. Synthesis of Mono 3



triblock copolymer was measured as $M_n = 28\,000$ Da, PDI = 1.2 (Figure 2).

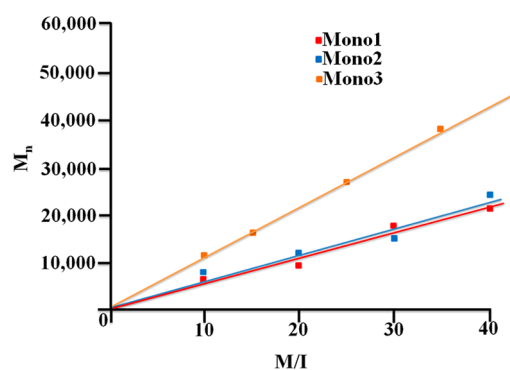
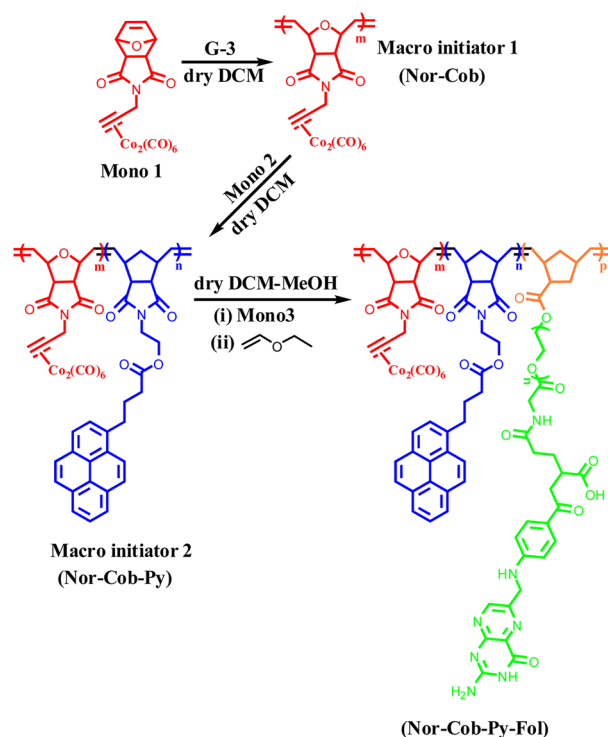
■ RESULT AND DISCUSSION

Monomers Synthesis. Toward the motivation of making a norbornene based copolymer with dual-imaging motifs in the monomers, **Mono 1–3**, were designed and synthesized as shown in Scheme 1–3. The formation of **Mono 1**, **Mono 2**, and **Mono 3** were confirmed by ^1H NMR and ^{13}C NMR spectroscopy. The synthesis with three steps of **Mono 1** was characterized using ^1H NMR and ^{13}C NMR spectroscopy techniques. In case of **2**, the propargylic proton appeared at $\delta = 2.1$ ppm in CDCl_3 (Figure S3) and after attachment to the cobalt that same proton shifted to the

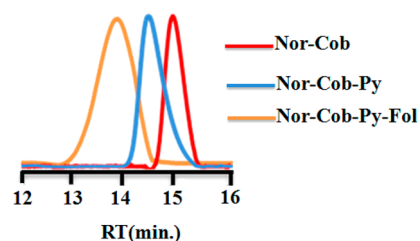
$\delta = 6.0$ ppm (Figure S5) which clearly confirmed the binding of cobalt carbonyl to the terminal alkyne groups (Figure S5). The ^{13}C NMR spectrum also clearly supported the formation of product as a new peak arose at $\delta = 200$ ppm (Co–CO) (Figure S6). The synthesis of **Mono 2** was also a two step process starting from commercially available exo-5 norbornene carboxylic anhydride. The anhydride was reacted with ethanol amine to get **3** as a pure white crystalline product (Scheme 2). This product upon reaction with pyrene butyric acid by using DCC, DMAP gave **Mono 2**. The formation of product was confirmed by NMR spectroscopy technique (Figure S9, S10). To make the system water-soluble, we synthesized **Mono 3**. To attach the folate moiety (Scheme 3), first we prepared amine terminated

Table 1. Homopolymerization of Mono 1–3 with Different M/I Ratios

run	poly	[M:I]	M_n (targeted)	M_n (GPC)	PDI
1	HP-Cob	10	5000	6000	1.04
2	HP-Cob	20	10000	9000	1.03
3	HP-Cob	30	15000	17000	1.07
4	HP-Cob	40	20000	22000	1.1
5	HP-Py	10	4700	7000	1.05
6	HP-Py	20	9500	11000	1.04
7	HP-Py	30	14300	15500	1.09
8	HP-Py	40	19080	23000	1.09
9	HP-Fol	10	12700	11000	1.12
10	HP-Fol	15	19050	15000	1.15
11	HP-Fol	25	31750	26000	1.19
12	HP-Fol	35	44450	37000	1.25

**Figure 1.** M_n versus M/I plot for three different monomers (1–3).**Scheme 4. Synthesis of Triblock Copolymer (Nor-Cob-Py-Fol) by Using Grubbs' Third Generation Catalyst (G-3)**

nor-peg (7). For that we synthesized Boc protected glycine (4) (Scheme 3). Boc anhydride was used to block the amine group of the glycine. The boc protected glycine (1.05 equiv) was further

**Figure 2.** GPC chromatogram of triblock copolymer (Nor-Cob-Py-Fol). **Macroinitiator 1** (Nor-Cob) $M_n = 8000$ Da (PDI = 1.04) ($m = 15$), **Macroinitiator 2** (Nor-Cob-Py) $M_n = 17000$ Da (PDI = 1.09) ($n = 19$), Final triblock copolymer (Nor-Cob-Py-Fol) $M_n = 28000$ Da, (PDI = 1.2) ($p = 10$).

reacted with peg in THF (1 equiv) ($M_w = 650$ Da) in the presence of DCC, DMAP, gave the amine terminated peg (5). This molecule was precipitated in cold ether for three times to get white sticky material as product (5) which was confirmed by ^1H NMR spectroscopy technique. (Figure S13) The free $-\text{OH}$ group present at the end of peg motif of compound 5 was functionalized to exonorbornene carboxylic acid by using DCC and DMAP. (Scheme 3) The product was precipitated in cold hexane to get the boc protected Nor-peg amine (6). (Figure S14) The deprotection of Nor-peg-amine boc (6) was done by using TFA. The formation of product (7) was confirmed by the disappearance of the characteristics boc methyl proton at $\delta = 1.39$ ppm peak (Figure S15). After successful synthesis of amine terminated nor peg (7), folic acid was reacted to it by using DCC and DMAP (Scheme 3) to get Nor-Peg-Folate (Mono 3) which was highly water-soluble. The formation of product was characterized by ^1H NMR spectrum (Figure S16), where the entire characteristic peaks were appeared.

After the successful synthesis of monomers, their polymerization conditions were explored. A series of homopolymers were produced by using Grubbs' third generation catalyst (G-3) with different feed ratio to evaluate the livingness of the polymerization (Table 1). It was observed that the polymerizations were well controlled (Figure 1), resulting in narrow polydispersity index (PDI), with good yield (70%–80%).^{11,13} After establishing the homo polymerization conditions for all the monomers, the triblock copolymerization (Scheme 4) was carried out by using Grubbs' third generation catalyst (G-3) at room temperature in dry DCM solvent by sequential addition of Mono 1–3. The polymerization was monitored by ^1H NMR spectroscopy. The molecular weights of the **Macroinitiator 1** (Nor-Cob, $M_n = 8000$, PDI = 1.04), **Macroinitiator 2** (Nor-Cob-Py, $M_n = 17000$, PDI = 1.09), and the final triblock copolymer (**Nor-Cob-Py-Fol**, $M_n = 28000$, PDI = 1.2) were measured in GPC by using poly(methyl methacrylate) standards. The shifting in GPC traces (Figure 2.) clearly indicated the formation of triblock copolymer (Nor-Cob-Py-Fol). Also, the formation of Nor-Cob-Py-Fol was confirmed through ^1H NMR spectroscopy (Figure S17). This final polymer was highly water-soluble. The attachment of cobalt carbonyl to the alkyne group was confirmed by I.R. spectrum (Figure S18). The I.R. spectrum of 2 shows the stretching frequency around 2126 cm^{-1} corresponding to acetylene moiety, which was completely disappeared and three new band was observed at 2097 , 2056 , and 2020 cm^{-1} corresponding to the metal–carbonyl group.¹³ After confirming the formation of **Nor-Cob-Py-Fol**, its thermal stability was measured using Thermo gravimetric analysis (TGA). TGA of the **Nor-Cob-Py-Fol**, performed at a heating rate of $10\text{ }^\circ\text{C}/\text{min}$ under nitrogen atmosphere. The first degradation point was observed at $220\text{ }^\circ\text{C}$

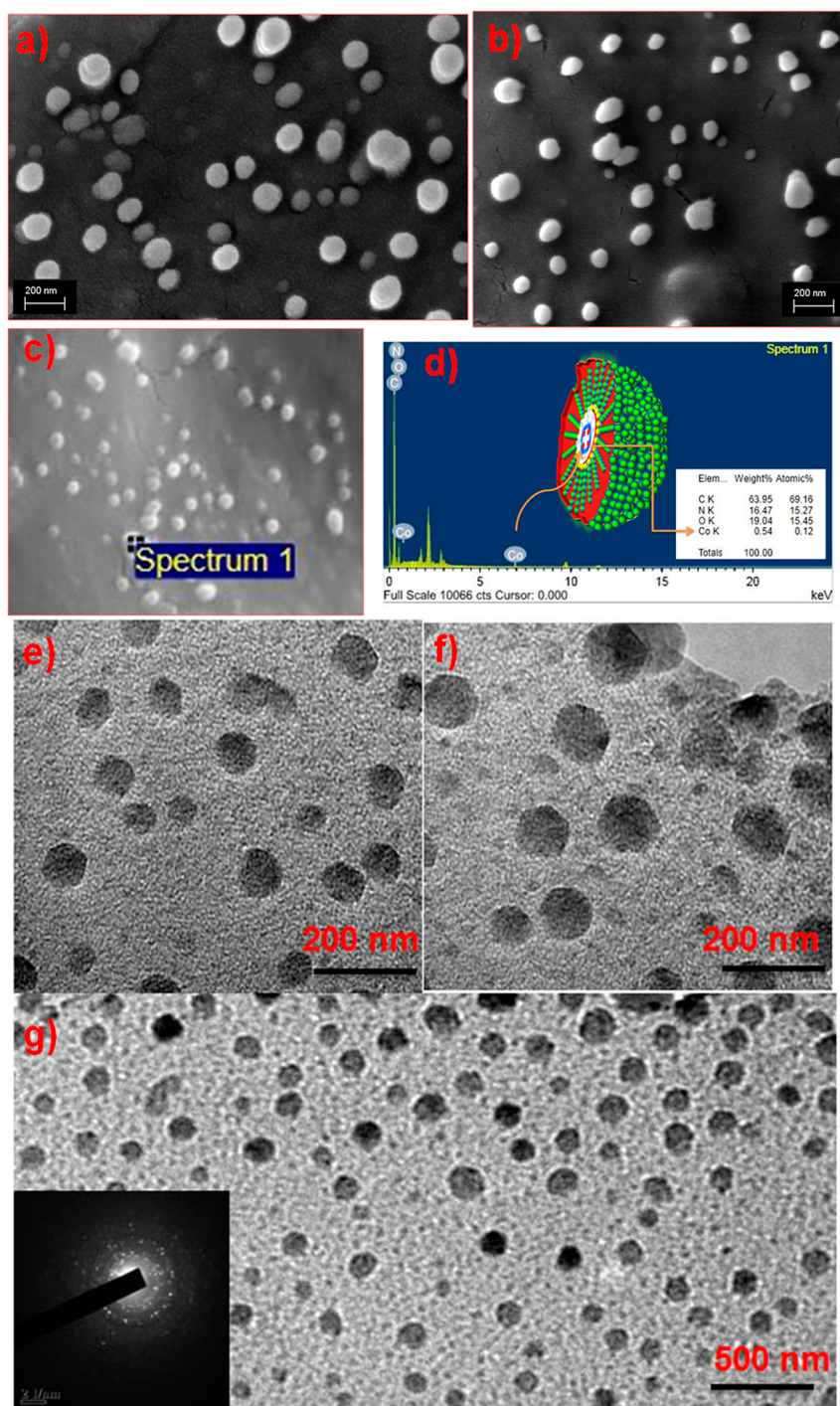


Figure 3. (a, b). SEM images of Nor-Cob-Py-Fol, (c, d). EDX analysis of final triblock copolymer (Nor-Cob-Py-Fol), (e, f, g) TEM images of Nor-Cob-Py-Fol.

(Figure S19). It was also observed that around 30% of degradation clearly confirmed the degradation of cobalt unit from the polymeric backbone. It was matching with the previously reported literature,³² and also confirmed the cobalt attachment to the polymer.

From the complex architecture of **Nor-Cob-Py-Fol**, it was obvious that the copolymer was amphiphilic in nature, so dynamic light scattering (DLS) analysis was done in water to measure the size of the nanoaggregates. The size (diameter) of the aggregates was around 160 nm with 0.275 PDI (Figure S20). The morphology of the aggregate was determined by SEM (scanning

electron microscope). A spherical morphology was observed with diameter 100 nm. (Figure 3a,b). The same spherical morphology having the size range 100 nm was observed in TEM as well. (Figure 3e–g). It was interesting that due to the presence of Co^{2+} inside the nanoaggregates, even without any contrast agent, the aggregates were dark under the electron beam. We envisaged that in the presence of polar environments, for example, under aqueous condition, **Nor-Cob-Py-Fol** would self-assemble into nanoaggregate where the hydrophilic peg-folate would be at the corona whereas the hydrophobic pyrene as well as Co^{2+} would be buried inside the core. It was interesting to note

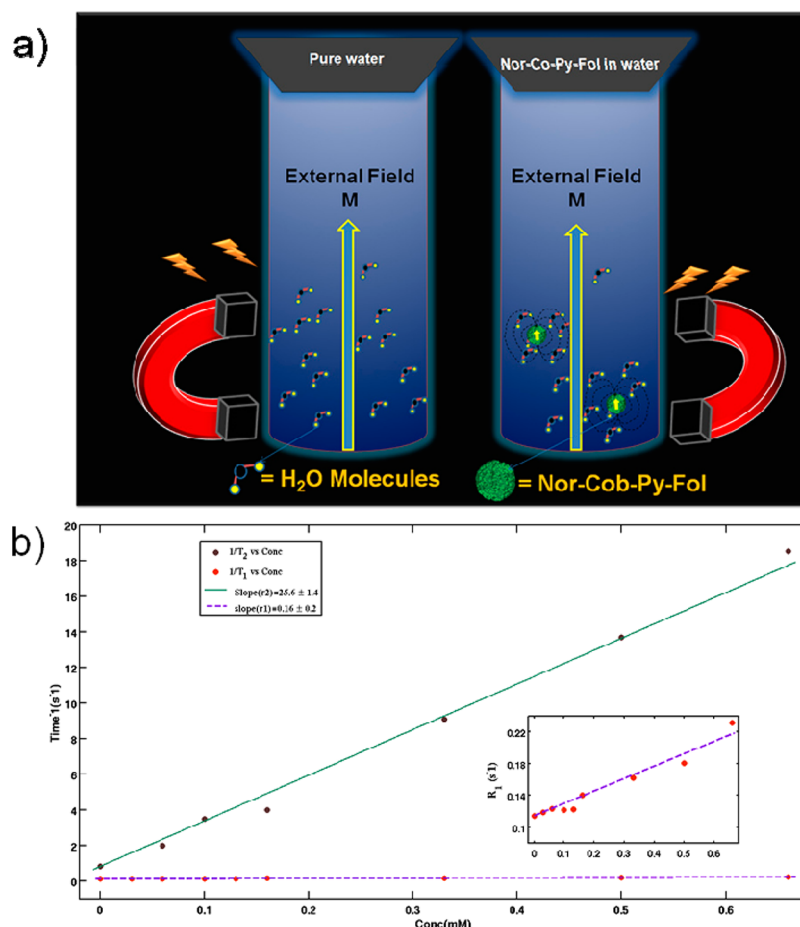


Figure 4. (a) Cartoon representation of water molecule behavior in the presence of Magnetic Copolymer (Nor-Cob-Py-Fol) (b) Transverse relaxation rates ($1/T_2$) and longitudinal relaxation rates ($1/T_1$) versus concentration of final triblock copolymer (Nor-Cob-Py-Fol).

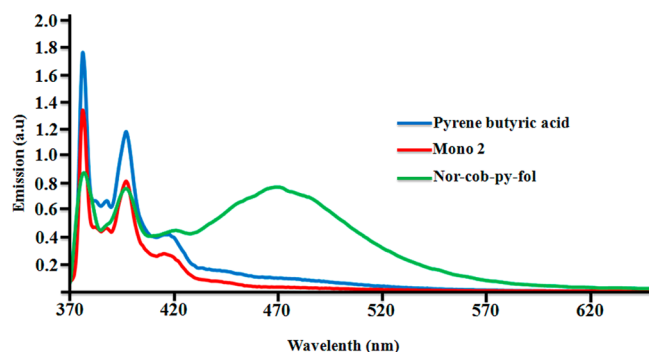


Figure 5. Emission spectra of pyrene butyric acid (blue), Mono 2 (red), and Nor-Cob-Py-Fol (green) at the same concentration ($10 \mu\text{M}$).

from EDX experiment showed that all particular spherical micelles were containing the cobalt unit, (Figure 3c,d), which proves our hypothesis. Next to prove the stability of our nanoaggregate, DLS study was performed to the solution containing 1 mg of Nor-Cob-Py-Fol in 1 mL of PBS buffer. The solution was kept for 7 days. DLS analysis was done for each day to monitor the change in the size of the nanoaggregate. Interestingly, the size of nanoaggregate was almost same for all 7 days (Figure S22). This suggested the stability of the nanoaggregate for a long period.

Next, to prove the Nor-Cob–Py-Fol nanoaggregates as a potential MRI agent, relaxivity measurements were performed.

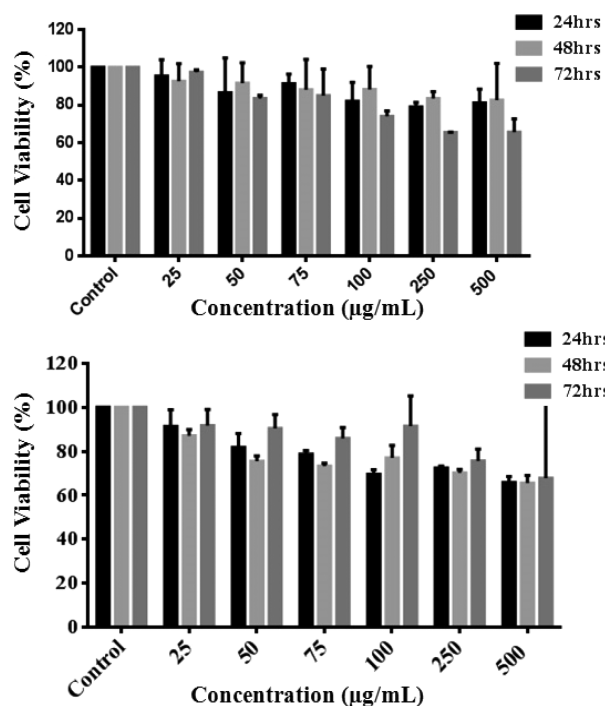


Figure 6. Cell viability assay of Nor-Cob-Py-Fol nanoaggregate on HeLa wt cells and HEK 293 cells.

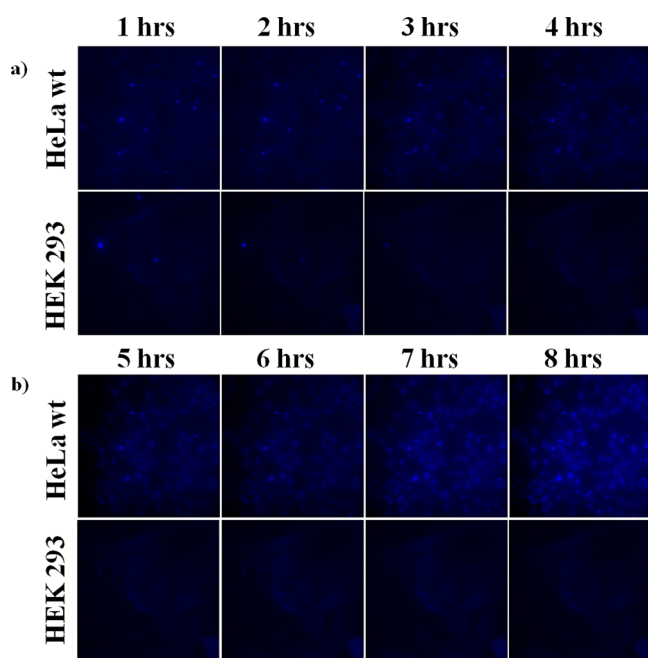


Figure 7. Live cell image of Nor-Cob-Py-Fol block copolymer on (a) HeLa wt. (Supporting Information, Video 1) and (b) HEK 293 cell lines (Supporting Information, Video 2).

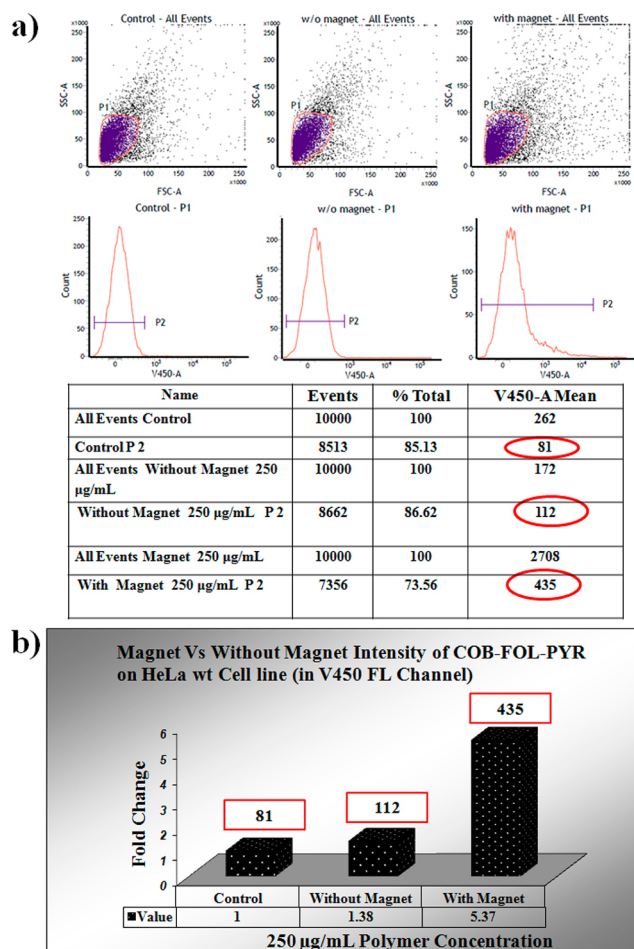


Figure 8. Magnet versus without magnet intensity of (a) Nor-Cob-Py-Fol and (b) on HeLa wt. cell line (in V450 FL channel).

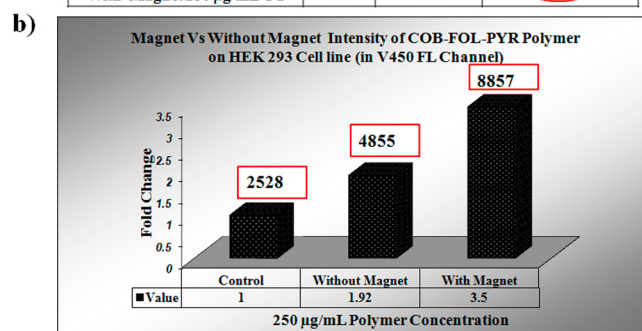
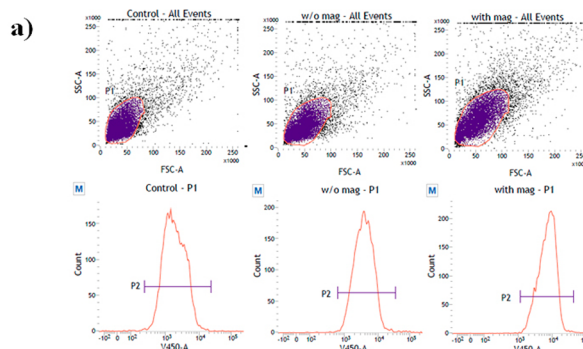


Figure 9. Magnet versus without magnet intensity of (a) Nor-Cob-Py-Fol and (b) on HEK 293 cell line (in V450 FL channel).

All relaxation studies were performed on a standard bore Bruker 500 MHz Avance III spectrometer at room temperature. We have made NMR samples of seven different concentrations (in millimolar) of synthesized final copolymer, dissolved in a mixture of H₂O and D₂O, taken in 1:5 ratios. We applied conventional inversion recovery and CPMG pulse sequences on water proton in order to study respectively T_1 and T_2 relaxation of water peak, affected due to the presence of polymer in aqueous medium. All experimental data were fitted by using Matlab programs.

Both T_1 and T_2 values were found to be decreasing with increasing concentration. But the relative changes of T_2 values with respect to concentrations were much more prominent than the relative change of T_1 values.

The $1/T_2$ (R_2) and $1/T_1$ (R_1) values were plotted in same graph with respect to concentrations. The behavior of experimental data was found to be linear and was fit with straight line functions given by the following equations.

$$1/T_1 = 1/(T_1)_0 + r_1 C$$

$$1/T_2 = 1/(T_2)_0 + r_2 C$$

where $1/(T_1)_0$ and $1/(T_2)_0$ were the longitudinal and transverse relaxation rate of the sample without any polymer solute (only 1:5 H₂O and D₂O mixture) and r_1 and r_2 were the relaxivity constants of T_1 and T_2 process respectively, measured from the slope of two straight lines. In this case, r_2 is 25.6 mmol⁻¹s⁻¹, much higher than the r_1 , which is 0.16 mmol⁻¹s⁻¹.

Super paramagnetic materials are more advantageous over paramagnetic system since a single particle of super paramagnetic

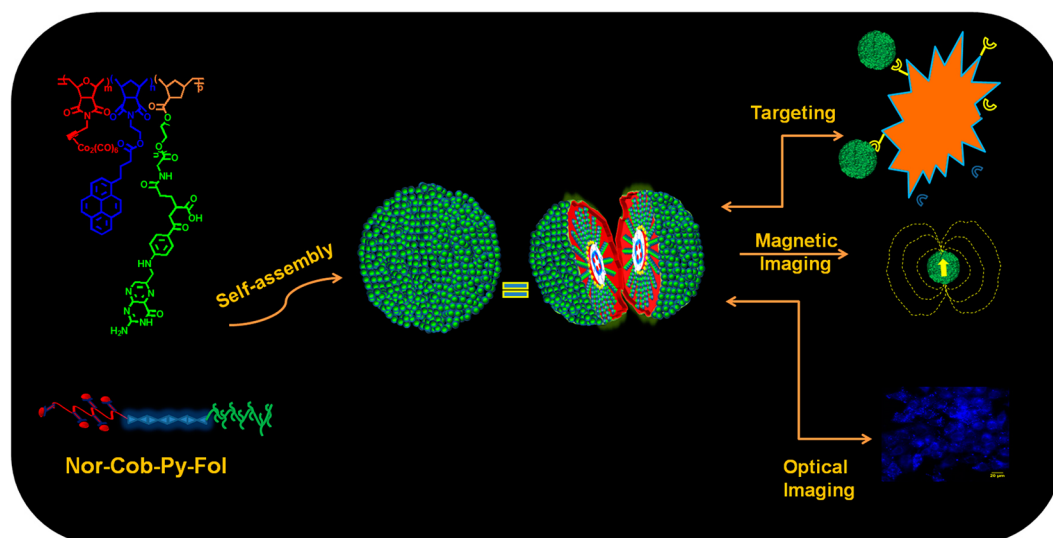


Figure 10. Cartoon representation of self-assembly of **Nor-Cob-Py-Fol** and its potential application as a dual-imaging agent.

materials bears a huge magnetic moment than the paramagnetic one.³³ Now the efficiency of contrast agent that accelerate the relaxation of H₂O proton is defined by the equation

$$R_{1,2} = R_{1,2}^0 + r_{1,2}C$$

where $R_{1,2}$ (unit s⁻¹) is the respective T_1 or T_2 proton relaxation rate in the presence of the contrast agent, $R_{1,2}^0$ is the relaxation rate in the absence of contrast agent, and C is the contrast agent's concentration (unit mM). The constant of proportionality $r_{1,2}$ (unit s⁻¹ mM⁻¹) is called relaxivity and is a measure of how much the proton relaxation rate is increased per unit of concentration of contrast medium. The enhancement of r_2/r_1 value is actually denoted the contrast efficiency of the magnetic material as contrast agent.

Higher value of the ratio always demonstrates the high contrast efficiency (T_2 weighted MRI imaging). There are several reports on T_2 weighted contrast agent based on the nano particle based systems, for example, Fe₃O₄ and Co²⁺ systems where actually a T_2 response image with varying concentration has been demonstrated.¹⁶ In general, a nanoparticle system, dispersed in solvent, affects the relaxivity of the water proton. It is well-known fact that poly(ethylene glycol) (PEG) coated nanoparticle system is even better as the hydrophilicity of molecule can give a better accessibility of water molecule to the paramagnetic center, which contributes greatly to the contrast efficiency of the magnetic particle.³⁴ So it is always better to have a water-soluble/dispersible magnetic system which can show a better efficiency for becoming a contrast agent.^{34–37} But achieving water solubility in small molecular systems is always an issue. Hence a polymeric system can act as a better system over nano particle as it can give a highly soluble/dispersible material by simply changing the feed ratio of poly(ethylene glycol) moiety that will produce high contrast efficiency. So keeping this in mind we investigated the diagnostic capability of our system by measuring the nuclear relaxivities r_1 (longitudinal) and r_2 (transverse). The measurement of relaxation of H₂O was done by varying the final polymeric concentration, where we observed the steady decrease of transverse relaxation time (T_2) with increasing the polymeric concentration; whereas the response on T_1 (longitudinal relaxation) of the same final copolymer (**Nor-Cob-Py-Fol**) having same concentration was negligible (Figure 4b). The efficiency of Co²⁺ metal as negative contrast agent is well-

known^{6,8} and in our system also the transverse relaxivity ($r_2 = 25.6 \text{ mmol}^{-1}\text{s}^{-1}$) is fully dominating over the longitudinal relaxivity ($r_1 = 0.16 \text{ mmol}^{-1}\text{s}^{-1}$) which is clearly proving the system as a T_2 weighted MRI contrast agent. Now this high r_2/r_1 ratio (160) at lower concentration of our polymeric nano carrier may be attributed to the high water solubility as that will give the water molecule a better access to magnetic center of the polymeric system (Figure 4a) and as well as at lower concentration of polymer, the amount of Co²⁺ present in the solution will be more compared to the nano particle system with same concentration, as a single polymeric chain is consisting of more number of Co²⁺ metal. Uniformity in aggregation also may be a cause for high relaxivity as aggregation causes to increase the T_2 markedly¹⁶ and also the saturation magnetization of cobalt is very high which can give larger effect on proton relaxation, leading to improve MRI contrast.^{38,16c}

$1/T_2$ (R_2) behavior could probably be better explained by using a parabolic equation. However, we would like to emphasize the usefulness of super paramagnetic cobalt as a useful T_2 weighted contrast agent compared than that of T_1 weighted contrast agent. Therefore, a linear fit was chosen to highlight the efficiency of r_2 relaxivity behavior.

After the successful demonstration of **Nor-Cob-Py-Fol** nanoaggregate as superior material having high r_2/r_1 values, its photo physical studies were performed to prove its dual imaging capabilities. The fluorescence emission spectrum of **Mono 2** in DCM showed three characteristic monomer emission peaks at 375 nm, 397 and 417 nm. The same was observed for pyrene butyric acid as well. No stacking was observed at the monomeric level in micro molar concentration (μM) concentration. The same concentration (10 μM) of nanoaggregate (**Nor-Cob-Py-Fol**) in water showed all characteristic monomeric emission in addition to that a new featureless emission peak centered at 475 nm (Figure 5) also observed, which clearly indicated the strong interaction of pyrene moiety at the excited state due to the constrained structure of norbornene backbone.²⁶ To check the emission stability of our nanoaggregate, we measured the quantum yield of the nanoaggregate in PBS for 7 days. Interestingly, the relative quantum yield did not show any change within 7 days (Figure S23). To demonstrate the advantage of our nanoaggregate (**Nor-Cob-Py-Fol**) in terms of fluorescence emission in water compared to monomeric pyrene,

quantum yield was measured for both monomeric pyrene and nanoaggregate in water. 15% quantum yield was observed for nanoaggregate compare to 1.1% quantum yield of monomeric pyrene butyric acid in water. This clearly suggested that in nanoaggregate, due to hydrophobic core inside micelles make the system stable and highly emissive in water itself (Figure S24).

After performing relaxivity as well as photophysical studies, experiments at cellular level were performed. For *in vitro* cytotoxicity study, HeLa wt cells (human cervical cancer cell line) and HEK 293 cells (human embryonic kidney cells) were maintained in MEM (minimum essential medium) containing with 10% fetal bovine serum (FBS), penicillium (100 U/mL), and streptomycin (100 $\mu\text{g}/\text{mL}$) were incubated at 37 °C in 5% CO₂ environment according to ATCC recommendations. Cells were seeded in 96-well plates at a density of 1×10^4 cells per well and grown for 24 h.

Cells were exposed with serial dilutions of various drug concentrations (25 to 500 $\mu\text{g}/\text{mL}$) of **Nor-Cob-Py-Fol** nanoaggregate at 37 °C. The cytotoxicity of **Nor-Cob-Py-Fol** nanoaggregate on HeLa wt cells and HEK 293 cells were assessed by the 3-(4, 5-dimethyl-2-thiazolyl)-2, 5-Diphenyltetrazolium bromide (MTT) assay having the concentration of 5 mg/mL in PBS (phosphate buffered saline). A fresh 20 μL solution of MTT was added to each well, followed by incubation for 4 h in 5% CO₂ at 37 °C. The medium in each well was removed and 100 μL of DMSO was added to each well and agitated for 15 min. The absorbance of the purple colored solution was measured at 525 nm by an ELISA plate reader (Bio Tek Instrument ELx 800). It was interesting to note that even after 72 h incubation, nanoaggregate showed very low cytotoxicity up to 250 $\mu\text{g}/\text{mL}$ concentrations. A slight toxicity was observed at the higher concentrations. This was considered very important that the dual imaging agents were well shielded by biocompatible Peg-Folate motif and hence very low cytotoxicity was observed (Figure 6.).

After proving the biocompatibility nature of **Nor-Cob-Py-Fol** nanoaggregate, cellular uptake studies were explored. The cellular uptake of **Nor-Cob-Py-Fol** nanoaggregate was studied in HeLa wt cells and HEK 293 cells. For cellular uptake experiment, live cell imaging were done for 8 h in 5% CO₂ at 37 °C at 250 $\mu\text{g}/\text{mL}$ in MEM (minimum essential medium).

From the live image experiments, it was clear that the HeLa wt cells were up taking more nanoaggregates compared to HEK 293 cells. From the live cell imaging, it was obvious that due to folate receptor, the internalization was stronger in HeLa wt cells rather than HEK 293 cells. Also, the blue emission from the pyrene motif confirmed the internalization of the nanoaggregates (Figure 7; Supporting Information Video 1 and 2).

To demonstrate the importance of the presence of Co²⁺ in our nanoaggregate the Mean Fluorescence Intensity (MFI) by BD FACSVerser™ instrument. The BD FACSVerser™ is a biophysical instrument which measures and analyses several physical properties of a cell and performs absolute counting of cells at a single cell level. In this experiment, once cells were getting suspended in a “flowing” fluid, based on certain parameters such as light scattering (FSC and SSC) and/or fluorescence emission, through laser interrogation, the results were interpreted.

To prove the magnetic field assisted internalization, an external magnetic field, was applied in the *in vitro* cell culture. HeLa wt cells and HEK 293 cells were seeded in 35 mm culture dish (concentration of 1×10^6 cells per dish) for 24 h. After 24 h incubation, **Nor-Cob-Py-Fol** nanoaggregate (having the concentration of 50 $\mu\text{g}/\text{mL}$ and 100 $\mu\text{g}/\text{mL}$) were applied to each

dish of two types of cell lines and were incubated for 24 h in 5% CO₂ at 37 °C. In both cell lines, the following conditions were maintained: (i) control, (ii) nanocarrier with magnetic field, and (iii) nanocarrier without magnetic field. After 24 h incubation, cells were washed with PBS (Phosphate buffered saline). Then the cells were collected by the cell scraper (Corning); centrifuged and resuspended in buffer (PBS). Then cells in suspension (approximately 1×10^5 cells per 500 μL buffer/flow tube) were distributed in each flow tube for analysis.

For flow cytometry analysis, V450 FL laser was selected because the excitation ($\lambda_{\text{ex}} = 408$ nm) and emission ($\lambda_{\text{em}} = 488$ nm) wavelengths were suitable for Pyrene. The histogram and column graph showed the changes in the mean fluorescence intensities (MFI) with the increasing of concentrations (i.e., 25, 50, 100, 250 $\mu\text{g}/\text{mL}$) of **Nor-Cob-Py-Fol** nanoaggregate in both cell lines (HeLa wt and HEK 293). A typical flow cytometry results by plotting MFI vs varying concentration of **Nor-Cob-Py-Fol** nanoaggregate in both HeLa wt and HEK 293 cell lines is shown in (Figure S27). The most exciting results were obtained from the histogram of the mean fluorescence intensities (MFI) in the presence of magnetic field. From the column graph, it was clear that a 1.58 fold increase in HEK 293 cell lines (Figure 9) and a 3.99 fold increase in HeLa wt cell lines (Figure 8) were observed in the presence of magnetic field.

The internalization was greater in the presence of magnetic field in both HEK 293 as well as HeLa wt cells. This result completely supported the magnetic nature of Co²⁺. It was further interesting to note that the internalization was 3.99 times in HeLa wt compare to the 1.58 fold in HEK 293. This also clearly demonstrated the importance of folate group which helped the internalization of nano carrier into HeLa wt cells more than the HEK 293 cells in the presence of magnetic field. Further the dual-imaging nature of the nano carrier was confirmed from the epifluorescence images. Because of the presence of pyrene, a blue emission was observed in the epifluorescence microscope images. It must be noted that the nucleus were not stained with any staining agents (e.g., DAPI). So the observed blue emission was due to the pyrene. Therefore, these chemical and biological results proved strongly that the **Nor-Cob-Py-Fol** nanoaggregate as a promising probe for biodualimaging (Figure 10.).

CONCLUSION

In conclusion, a norbornene based nanocarrier, **Nor-Cob-Py-Fol**, with magnetic targeting and dual-imaging (Fluorescence imaging and MRI) capabilities in a single polymeric system without using exogenous organic dyes or quantum dots has been reported. Cell viability studies eliminate long-term toxicity concerns. It is quite interesting to note that the nano-carrier is stable over more than a week under the aqueous conditions. This is only possible because of the covalent attachment of Co²⁺ to the polymer backbone. Thermo gravimetric analysis (TGA) confirms the 30% cobalt attachment to the polymeric backbone of **Nor-Cob-Py-Fol** nanoaggregate. The relaxivity study confirms that the system is T₂ weighted MRI contrast agent having unusually high relaxivity ratio values. Epifluorescence microscope studies showed that **Nor-Cob-Py-Fol** nanoaggregate is capable of optical imaging. Moreover, the targeted accumulation of this dual-imaging agent is observed due to the presence of folate functionality. Hence, our system has the potential to be the one of the best contrast agents known to the practitioners of dual-imaging.

■ ASSOCIATED CONTENT

Supporting Information

The Supporting Information is available free of charge on the ACS Publications website at DOI: 10.1021/acs.macromol.5b01716.

Experimental details for all monomers and their NMR characterization, MALDI–TOF analysis, and NMR of polymer, IR, DLS, TGA, photophysical study, quantum yield calculation, mean fluorescence intensity, and cellular uptake studies (PDF)

From the live cell imaging, it was obvious that due to folate receptor, the internalization was stronger in HeLa wt cells rather than HEK 293 cells. (AVI)

The blue emission from the pyrene motif confirmed the internalization of the nanoaggregates. (AVI)

■ AUTHOR INFORMATION

Corresponding Author

*E-mail: sraja@iiserkol.ac.in.

Notes

The authors declare no competing financial interest.

■ ACKNOWLEDGMENTS

S.M. thanks CSIR for the research fellowship, H.D. and I.C. thank CSIR, New Delhi, for research fellowships, R.S. thanks the Department of Science and Technology, New Delhi, for a Ramanujan Fellowship and DBT for funding. R.S., R.B., and J.D.S. thank IISER-Kolkata for providing the infrastructure and start up funding.

■ REFERENCES

- (1) Weissleder, R.; Pittet, M. J. Imaging in the era of molecular oncology. *Nature* **2008**, *452*, 580–589.
- (2) Weissleder, R.; Tung, C.-H.; Mahmood, U.; Bogdanov, A., Jr. *Nat. Biotechnol.* **1999**, *17*, 375–378.
- (3) Bouchard, L. S.; Anwar, M. S.; Liu, G. L.; Hann, B.; Xie, Z. H.; Gray, J. W.; Wang, X. D.; Pines, A.; Chen, F. F. *Proc. Natl. Acad. Sci. U. S. A.* **2009**, *106*, 4085.
- (4) Kim, D.-H.; Zeng, H.; Ng, T.; Brazel, C. S. *J. Magn. Magn. Mater.* **2009**, *321*, 3899–3904.
- (5) Bleul, R.; Thiermann, R.; Marten, G. U.; House, M. J.; Pierre, T. G.; St.; Hafeli, U. O.; Maskos, M. *Nanoscale* **2013**, *5*, 11385.
- (6) Evans, R.; Timmel, C. R.; Hore, P. J.; Britton, M. M. *J. Am. Chem. Soc.* **2006**, *128*, 7309–7314.
- (7) Comes Franchini, M.; Baldi, G.; Bonacchi, D.; Gentili, D.; Giudetti, G.; Lascialfari, A.; Corti, M.; Marmorato, P.; Ponti, J.; Micotti, E.; Guerrini, U.; Sironi, L.; Gelosa, P.; Ravagli, C.; Ricci, A. *Small* **2010**, *6*, 366.
- (8) Tsitovich, P. B.; Sperryak, J. A.; Morrow, J. R. *Angew. Chem., Int. Ed.* **2013**, *52*, 13997.
- (9) Bleul, R.; Thiermann, R.; Marten, G. U.; House, M. J.; Pierre, T. G.; St.; Hafeli, U. O.; Maskos, M. *Nanoscale* **2013**, *5*, 11385.
- (10) Ganivada, M. N.; Rao N, V.; Dinda, H.; Kumar, P.; Das Sharma, J. D.; Shunmugam, R. *Macromolecules* **2014**, *47*, 2703.
- (11) Lee, H.; Lee, E.; Kim, D. K.; Jang, N. K.; Jeong, Y. Y.; Jon, S. *J. Am. Chem. Soc.* **2006**, *128*, 7383.
- (12) Chung, H. J.; Lee, H.; Bae, K. H.; Lee, Y.; Park, J.; Cho, S.-W.; Hwang, J. Y.; Park, H.; Langer, R.; Anderson, D.; Park, T. G. *ACS Nano* **2011**, *5*, 4329.
- (13) AL-Badri, Z. M.; Tew, G. N. *Macromolecules* **2008**, *41*, 4173.
- (14) AL-Badri, Z. M.; Maddikeri, R. R.; Zha, Y.; Thaker, H. D.; Dobriyal, P.; Shunmugam, R.; Russell, T. P.; Tew, G. N. *Nat. Commun.* **2011**, *2*, 482.
- (15) Withey, A. B. J.; Chen, G.; Nguyen, T. L. U.; Stenzel, M. H. *Biomacromolecules* **2009**, *10*, 3215.
- (16) (a) Faucher, L.; Gossuin, Y.; Hocq, A.; Fortin, M.-A. *Nanotechnology* **2011**, *22*, 295103. (b) Shin, T.-H.; Choi, J.-S.; Yun, S.; Kim, II-S.; Song, H.-T.; Kim, Y.; Park, K. I.; Cheon, J. *ACS Nano* **2014**, *8*, 3393. (c) Parkes, L. M.; Hodgson, R.; Lu, L. T.; Tung, L. D.; Robinson, I.; Fernig, D. G.; Thanh, N. T. K. *Contrast Media Mol. Imaging* **2008**, *3*, 150. (d) Olatunde, A. O.; Cox, J. M.; Daddario, M. D.; Sperryak, J. A.; Benedict, J. B.; Morrow, J. R. *Inorg. Chem.* **2014**, *53*, 8311. (e) Pablico-Lansigan, M. H.; Hickling, W. J.; Japp, E. A.; Rodriguez, O. C.; Ghosh, A.; Albanese, C.; Nishida, M.; Van Keuren, E.; Fricke, S.; Dollahon, N.; Stoll, S. L. *ACS Nano* **2013**, *7*, 9040.
- (17) Davis, M. E.; Chen, Z.; Shin, D. M. *Nat. Rev. Drug Discovery* **2008**, *7*, 771–782.
- (18) Smith, A. M.; Mancini, M. C.; Nie, S. *Nat. Nanotechnol.* **2009**, *4*, 710–711.
- (19) Duncan, R. *Nat. Rev. Cancer* **2006**, *6*, 688–701.
- (20) Ahmed, E.; Morton, S. W.; Hammond, P. T.; Swager, T. M. *Adv. Mater.* **2013**, *25* (32), 4504–4510.
- (21) Rolfe, B. E.; Blakey, I.; Squires, O.; Peng, H.; Boase, N. R. B.; Alexander, C.; Parsons, P. G.; Boyle, G. M.; Whittaker, A. K.; Thurecht, K. J. *J. Am. Chem. Soc.* **2014**, *136*, 2413–2419.
- (22) Wadajkar, A. S.; Kadapure, T.; Zhang, Y.; Cui, W.; Nguyen, K. T.; Yang, J. *Adv. Healthcare Mater.* **2012**, *1* (4), 450–456.
- (23) Sung, H.-J.; Luk, A.; Murthy, N. S.; Liu, E.; Jois, M.; Joy, A.; Bushman, J.; Moghe, P. V.; Kohn, J. *Soft Matter* **2010**, *6*, 5196–5205.
- (24) Fuchs, A. V.; Gemmel, A. C.; Thurecht, K. J. *Polym. Chem.* **2015**, *6*, 868–880.
- (25) Küick, K. L. *Science* **2007**, *317*, 1182.
- (26) Gorodetskaya, I. A.; Gorodetsky, A. A.; Vinogradova, E. V.; Grubbs, R. H. *Macromolecules* **2009**, *42*, 2895–2898.
- (27) Rao N, V.; Ganivada, M. N.; Sarkar, S.; Dinda, H.; Chatterjee, K.; Dalui, T.; Das Sarma, J.; Shunmugam, R. *Bioconjugate Chem.* **2014**, *25*, 276–285.
- (28) Deshmukh, P.; Gopinadhan, M.; Choo, Y.; Ahn, S.-K.; Majewski, P. W.; Yoon, S. Y.; Bakajin, O.; Elimelech, M.; Osuji, C. O.; Kasi, R. M. *ACS Macro Lett.* **2014**, *3*, 462–466.
- (29) Louie, J.; Grubbs, R. H. *Angew. Chem., Int. Ed.* **2001**, *40*, 247.
- (30) Rao N, V.; Mane, S. R.; Kishore, A.; Das Sarma, J.; Shunmugam, R. *Biomacromolecules* **2012**, *13*, 221–230.
- (31) Mane, S. R.; Rao N, V.; Shunmugam, R. *ACS Macro Lett.* **2012**, *1*, 482–488.
- (32) Miinea, L. A.; Sessions, L. B.; Ericson, K. D.; Glueck, D. S.; Grubbs, R. B. *Macromolecules* **2004**, *37*, 8967.
- (33) Jaganathan, H.; Hugar, D. L.; Ivanisevic, A. *ACS Appl. Mater. Interfaces* **2011**, *3*, 1282–1288.
- (34) Duan, H.; Kuang, M.; Wang, X.; Wang, Y. A.; Mao, H.; Nie, S. *J. Phys. Chem. C* **2008**, *112*, 8127–8131.
- (35) Lee, H.; Lee, E.; Kim, D. K.; Jang, N. K.; Jeong, Y. Y.; Jon, S. *J. Am. Chem. Soc.* **2006**, *128*, 7383–7389.
- (36) Tong, S.; Hou, S.; Zheng, Z.; Zhou, J.; Bao, G. *Nano Lett.* **2010**, *10*, 4607–4613.
- (37) Yang, H.; Zhou, H.; Zhang, C.; Li, X.; Hu, H.; Wu, H.; Yang, S. *Dalton Trans.* **2011**, *40*, 3616–3621.
- (38) Lukanov, P.; Anuganti, V. K.; Krupskaya, Y.; Galibert, A.-M.; Soula, B.; Tilmaciu, C.; Velders, A. H.; Klingeler, R.; Buchner, B.; Flahaut, E. *Adv. Funct. Mater.* **2011**, *21*, 3583.